Article

Data Assimilation of the High-Resolution Sea Surface Temperature Obtained from the Aqua-Terra Satellites (MODIS-SST) Using an Ensemble Kalman Filter

Yasumasa Miyazawa [1,*], Hiroshi Murakami [2], Toru Miyama [1], Sergey M. Varlamov [1], Xinyu Guo [1,3], Takuji Waseda [1,4] and Sourav Sil [1]

[1] Japan Agency for Marine-Earth Science and Technology, Yokohama, Kanagawa 236-0001, Japan;
E-Mails: tmiyama@jamstec.go.jp (T.M.); vsm@jamstec.go.jp (S.M.V.); sourav@jamstec.go.jp (S.S.)

[2] Japan Aerospace Exploration Agency, Tsukuba, Ibaragi 305-8505, Japan;
E-Mail: murakami.hiroshi.eo@jaxa.jp

[3] Ehime University, Matsuyama, Ehime 790-8577, Japan; E-Mail: guo.xinyu.mz@ehime-u.ac.jp

[4] The University of Tokyo, Kashiwa, Chiba 277-8561, Japan; E-Mail: waseda@k.u-tokyo.ac.jp

* Author to whom correspondence should be addressed; E-Mail: miyazawa@jamstec.go.jp;
Tel.: +81-45-778-5518; Fax: +81-45-778-5707.

Abstract: We develop an assimilation method of high horizontal resolution sea surface temperature data, provided from the Moderate Resolution Imaging Spectroradiometer (MODIS-SST) sensors boarded on the Aqua and Terra satellites operated by National Aeronautics and Space Administration (NASA), focusing on the reproducibility of the Kuroshio front variations south of Japan in February 2010. Major concerns associated with the development are (1) negative temperature bias due to the cloud effects, and (2) the representation of error covariance for detection of highly variable phenomena. We treat them by utilizing an advanced data assimilation method allowing use of spatiotemporally varying error covariance: the Local Ensemble Transformation Kalman Filter (LETKF). It is found that the quality control, by comparing the model forecast variable with the MODIS-SST data, is useful to remove the negative temperature bias and results in the mean negative bias within −0.4 °C. The additional assimilation of MODIS-SST enhances spatial variability of analysis SST over 50 km to 25 km scales. The ensemble spread variance is effectively utilized for excluding the erroneous temperature data from the assimilation process.

1. Introduction

Sea Surface Temperature (SST) is one of the important geophysical variables, acting as a medium between atmospheric and oceanic variations through activation of coupling mechanisms [1]. The small scale SST field is characterized by many types of oceanic front variability. The high-resolution satellite SST observation data have been used for detection of the SST frontal variability. One of difficulty in using the high-resolution satellite SST is the noise of infrared radiometers due to the cloud effects [2,3].

Several methods have been developed to exclude the noise and recover the missing data due to noise. For example, temporal composite of the infrared sensors data is adopted to provide a high-resolution SST product for regional weather applications [4]. Spline interpolation, e.g., [5], optimum interpolation, e.g., [6], and empirical orthogonal functions, e.g., [7], are also used for reconstruction of the missing SST data. Statistical merging of infrared (higher-resolution and sensitive to clouds) and microwave (lower-resolution and cloud free) sensors data has been proposed to respond to the cloud noise problem [8,9]. All the methods mentioned above can be interpreted as the statistical interpolation of physical variables. Physical consistency in the reconstructed variables is indirectly guaranteed through proper specification of the statistical parameters associated with the interpolation.

Recent developments of oceanic data assimilation combined with numerical ocean models are fundamentally based on intensive use of satellite data including SST, e.g., [10]. A proper combination of advanced data assimilation methods and high-resolution ocean models could contribute to production of the noise-free SST analysis with a high resolution because dynamic interpolation of physical variables is one of important roles of the data assimilation. Though the dynamic interpolation using numerical ocean models requires much more computational resources than the statistical interpolation, it allows physical consistency in the reconstructed variables more directly than the statistical interpolation. The dynamic interpolation of remote sensing data by the data assimilation is not only limited on surface area of missing data but also works in a vertical direction. Estimation of the unobserved subsurface variables from the observed surface information (vertical projection; [11]) is also included in the aims of the oceanic data assimilation.

Most applications of the oceanic data assimilation have mainly used the satellite SST products that were carefully sampled for removing the noise. In this study, we aim to evaluate the feasibility of the relatively raw data prior to the rigorous sampling, which keep the high horizontal resolution of O (1 km) but potentially involve the noise. Careful treatment of the infrared sensors SST data including, cloud noise, is required for the effective data assimilation. As a first step, focusing on the SST front variability affected by the internal ocean dynamics, we examine the winter SST condition rather than the summer SST condition, in which the SST front tends to be undetectable due to increased solar insolation [12]. We adopt the Ensemble Kalman Filter (EnKF) [13], which may be suitable for the fine representation of the front variability, because EnKF allows spatiotemporally

varying 'flow-dependent' error covariance working to reasonably conserve the sharp front property without unrealistic smoothing, given that the model resolves the associated front variability [10].

This paper is organized as follows. Section 2 describes the data assimilation procedure and design of sensitivity experiments. The Local Ensemble Transformation Kalman Filter (LETKF) [14] is a main tool for the EnKF implementation, and the Moderate Resolution Imaging Spectroradiometer (MODIS) SST data are assimilated into an ocean model of the south of Japan. Section 3 discusses the results of the sensitivity experiments. Section 4 is devoted to a final conclusion.

2. Data Assimilation of Satellite Sea Surface Temperature

2.1. Ensemble Kalman Filter (EnKF) for the Kuroshio Variation South of Japan

We examine the assimilation effects of high-resolution SST data using an EnKF system developed for investigation of the Kuroshio variation south of Japan [10]. The EnKF system utilizes twenty members of ensemble simulations, calculated by a sigma-coordinate ocean circulation model covering a region south of Japan: 30°–35°N, 133°–140°E (Figure 1) with horizontal 1/36° resolution and 31 vertical levels, which was developed on the basis of a parallel calculation code of the Princeton Ocean Model (sbPOM) [15]. Note that sbPOM in this study does not use a second order baroclinic pressure gradient scheme used in our previous study [10] but uses a fourth order one [16]. The EnKF algorithm is based on the Local Ensemble Transformation Kalman Filter (LETKF) [11,17].

Figure 1. (**Left**): Positions of the observation data without Moderate Resolution Imaging Spectroradiometer (MODIS-SST). Thick lines: sea surface height anomaly, crosses: satellite sea surface temperature, triangles: *in situ* temperature, squares: *in situ* salinity. Contours denote iso-depth lines: 10, 20, 30, 40, 50, 100, 200, 500, 1,000, 2000, 3000, 4,000, and 5,000 m. (**Right**): Snapshots of MODIS-SST gridded on the model grid for visualization. Note that the assimilated data with approximately 1 km resolution themselves are not gridded on the model grid of 1/36° resolution. Interval of thin (thick) contours is 1 °C (5 °C). (**a**,**b**): 14 February 2010. (**c**,**d**): 20 February 2010. (**e**,**f**): 26 February 2010. The abbreviations in (**f**) represents locations: KC (Kii Channel) and II (Izu Islands).

(**a**)   (**b**)

Figure 1. *Cont.*

(c)

(d)

(e)

(f)
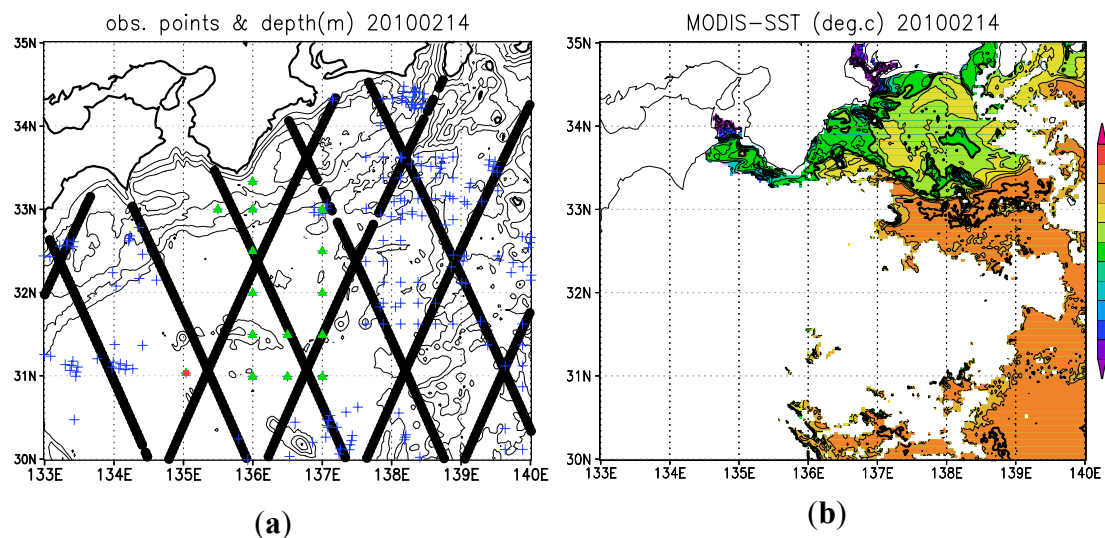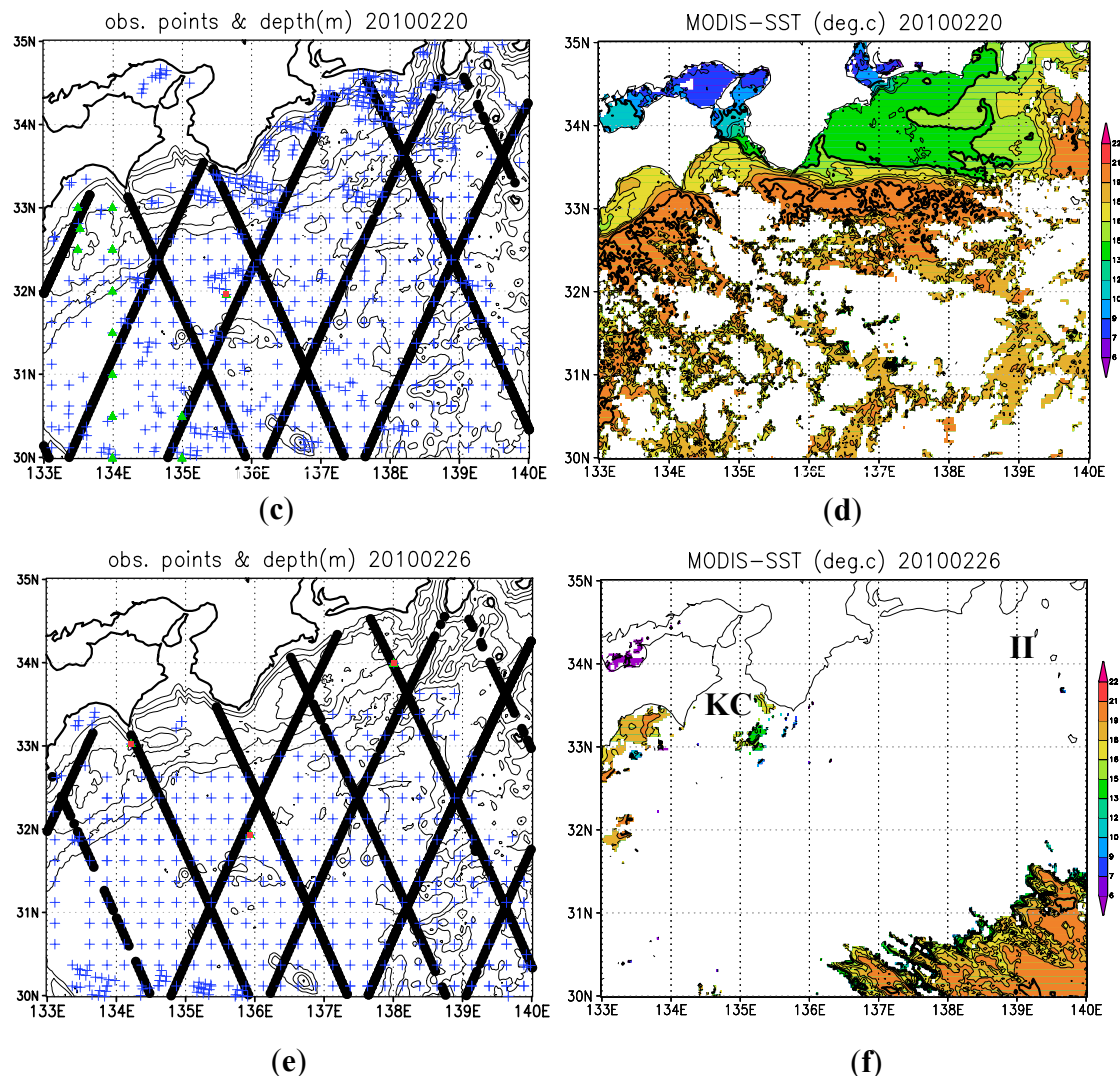
The original EnKF system [10] assimilates sea surface height anomaly (SSHA) obtained from two altimeter satellites: Jason-1 and -2, satellite SST, and *in situ* temperature and salinity with a time interval of two days, e.g., Figure 1 (a,c,e). The satellite SST data come from two types of sensors: Advanced Very High Resolution Radiometer (AVHRR) with relatively high horizontal resolution of 1 km and the Advanced Microwave Scanning Radiometer—Earth Observing System (AMSR-E) with relatively moderate resolution of 25 km. The SST data from the former one are retrieved using Multi Channel SST (MCSST) algorithm [18] and resampled by the Fleet Numerical Meteorology and Oceanography Center (FNMOC) and the Naval Oceanographic Office (NAVOCEANO). As a result of resampling with carefully designed quality control algorithms, spatial resolution of MCSST becomes relatively coarse, 8 km [19]. We call them the resampled MCSST (RMCSST). A typical distribution of RMCSST is depicted in near-shore regions of Figure 1(c). AMSR-E points show a gridded-like distribution in offshore region especially shown in Figure 1(e). We expect that the high-resolution MODIS-SST data (Figure 1(b,d,f)); their detail is described in Section 2.2) to show more detailed features of the surface oceanic condition than the observation data indicated in Figure 1(a,c,e). In this

study, the EnKF system assimilates only sea surface height anomaly and satellite SST, and the *in situ* data are not assimilated into the system but used only for validation of the assimilation products.

The LETKF system assimilates the observation data during a target period from 8 February to 28 February 2010 [10]. Parameters of LETKF are summarized in Table 1, for reader reference. Detail on the parameters is described in our previous paper [10]. The original EnKF system involves a quality control method of the assimilation data as following:

$$Exclude \quad SST^o(SSHA^o) \quad if \quad \left| SST^o(SSHA^o) - SST^f(SST^o) \right| > 10°C(2m)$$
(1)

where $SST^o(SSHA^o)$ and $SST^f(SSHA^f)$ denote observation and forecast values of $SST(SSHA)$, respectively.

Table 1. Parameters used in Local Ensemble Transformation Kalman Filter (LETKF).

Parameters	Values
Horizontal localization scale (σ_{obs}; number of grids)	12 (1/3°)
Vertical localization scale (σ_{obsv}; m)	2000
Covariance inflation parameter (%)	21
Observation error of sea surface height anomaly (m)	0.2
Observation error of sea surface temperature (°C)	1.0
Time window of sea surface height anomaly (day)	±4
Time window of sea surface temperature (day)	±1
Time interval of LETKF (day)	2

2.2. Moderate Resolution Imaging Spectroradiometer (MODIS) Sensors—SST

The MODIS SST data are additionally assimilated into the model in this study. The MODIS sensors are major sensors aboard the Terra and Aqua satellites launched by National Aeronautics and Space Administration (NASA) in December 1999 and May 2002, respectively. They are viewing the entire Earth's surface every 1 to 2 days, acquiring data with approximately 1 km resolution.
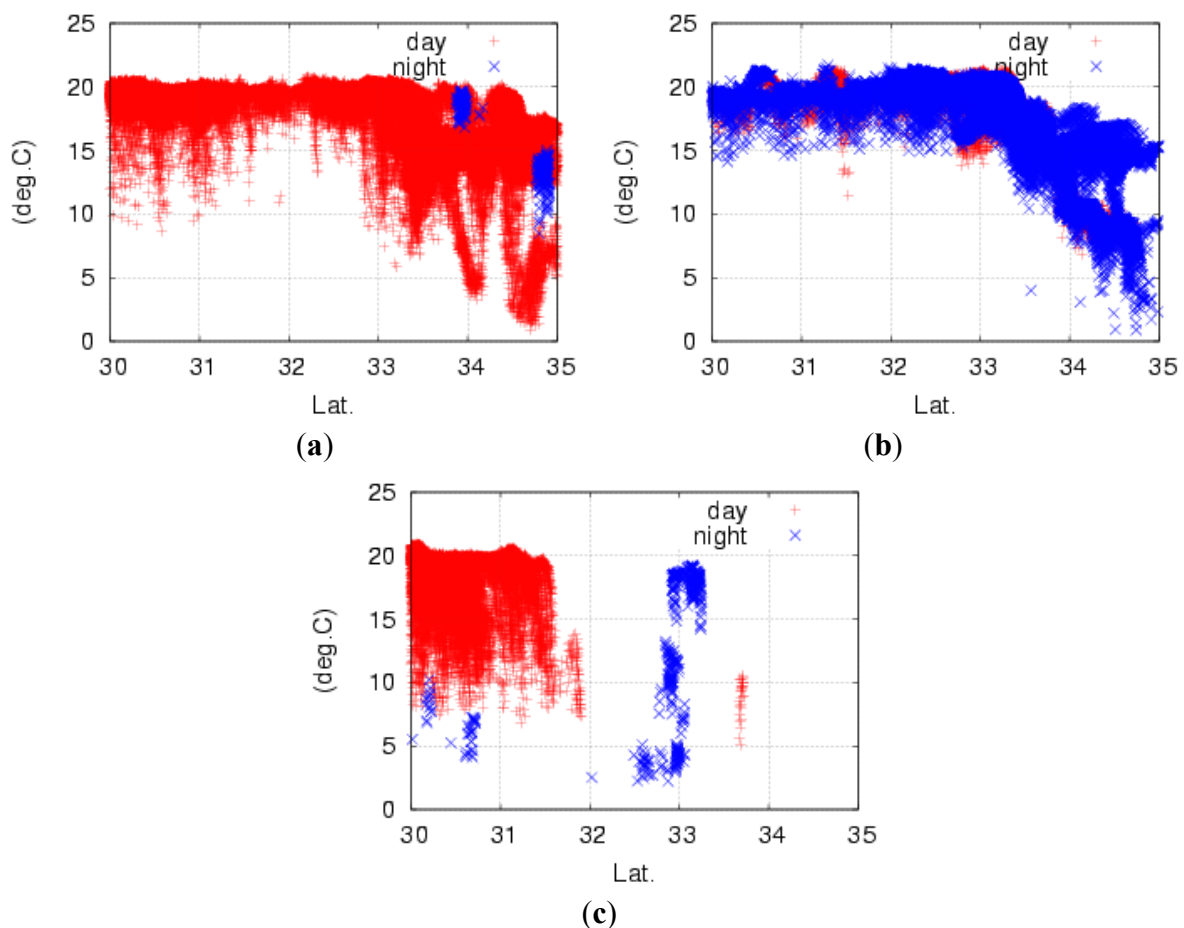
The raw data are directly received from the satellites by Tokai University Research & Information Center, and then sea surface temperature is retrieved by Earth Observation Research Center of Japan Aerospace Exploration Agency using an algorithm: MODIS Near-real-time Algorithm Version 3, developed by Hosoda *et al.* [2]. Root Mean Square Error (RMSE)s for *in situ* data under the clear sky condition are 0.70 K/0.65 K for daytime (Aqua/Terra) and 0.65 K/0.66 K for nighttime, respectively. The retrieval error could be enhanced under the weak wind condition. The aerosol contamination also could be a possible cause of the error. One of most serious problems in the retrieval of SST is the cloud contamination as it causes significantly negative noise in the SST fields. The errors of SST including near-cloud areas could be as poor as 2–5 °C [3]. Though more sophisticated cloud screening algorithms are recently proposed, e.g., [3], we assimilate the MODIS-SST data masked by the traditional cloud screening algorithm (See Table 1 in [2]), which cannot completely remove the pixels contaminated by the clouds [3].

Addition of MODIS-SST into the assimilation data archive considerably increases spatial density of sea surface temperature data (Figure 1(b,d,e)). Atmospheric conditions including the existence of clouds affect the data availability. Detailed front structures associated with the Kuroshio variations are clearly represented by MODIS-SST in the case of clear sky condition (Figure 1(d)). Open ocean south

of 32 °N is characterized by relatively warm temperatures around 18 °C. In contrast, unrealistic low temperature data are found in a case of cloudy sky conditions (see around the lower right corner of Figure 1(f)).

A scatter plot of MODIS-SST in a relatively clear sky condition (Figure 2(b)) indicates a shape of SST gradient from open ocean (higher values around 18 °C at lower latitudes) to coastal seas (lower values around 7 °C at higher latitudes), which is distorted in cloudy sky conditions (Figure 2(a,c)). Variability of SST at each latitude is relatively large even in the clear sky case and its range exceeds 5 °C (Figure 2(b)). Comparison of the plots between clear (Figure 2(b)) and cloudy sky (Figure 2(a,c)) conditions suggests that a large part of the noise is characterized as lower temperature bias [3]. Note that we simultaneously assimilate both of them at the analysis time since Figure 2 does not show any systematic difference between daytime and nighttime SST.

Figure 2. Scatter plots of sea surface temperature at each latitude used for the analyses on 14 February 2010 (**a**), 20 February 2010 (**b**), and 26 February 2010 (**c**). Crosses: daytime, X signs: night time.

(a)

(b)

(c)

2.3. Data Assimilation Experiments

We investigate effects of a quality control method that excludes erroneous sea surface temperature values using a following algorithm:

$$Exclude \quad SST^o \quad if \quad SST^o - SST^f < -m \quad or \quad SST^o - SST^f > +p \tag{2}$$

where SST^o and SST^f denote MODIS-SST and ensemble mean forecast SST values, respectively. Positive values m and p are control parameters. At first, we assimilate MODIS-SST using the default quality control algorithm (1) with a moderate criterion: m = 10 and p = 10 (mqc) and compare the result with a reference case with no MODIS-SST data assimilation (NO-MODIS). We also check an effect of larger observation error for MODIS-SST, 5 °C, in which the value is roughly suggested from Figure 2, than default value of 1 °C (5degerr). Then we examine five cases of different m and p values: (1) m = 3 p = 4 (m3p4), (2) m = 2 p = 2 (m2p2), (3) m = 1 p = 2 (m1p2), (4) m = 2 p = 10 (m1), and (5) m = 1 p = 10 (m2). The acceptable range of MODIS-SST could have asymmetric negative (m) and positive (p) maximum differences for the ensemble mean forecast SST, because the raw data include unrealistic low values due to the cloud effects (Figure 2). We call the four cases mentioned above (m2p2, m1p2, m1, m2) the static quality control cases.

To utilize the information from the ensemble simulation, we conduct an additional four experiments with a different type of criterion, including the ensemble spread information (the dynamic quality control cases): (1) m = 2*sprd* p = 2*sprd* (dqc.m2p2), (2) m = *sprd* p = 2*sprd* (dqc.m1p2), (3) m=2*sprd* p=10 (dqc.m2), and (4) m=*sprd* p=10 (dqc.m1), where $sprd = \sqrt{\sum_{i=1}^{K} (x_i - \bar{x})^2 / K}$, $\bar{x} = \sum_{i=1}^{K} x_i / K$, K = 20 is ensemble size, and x_i denotes SST of an ensemble member forecast. The dynamic quality control tends to assimilate MODIS-SST more in cases of the relatively large forecast errors, because the ensemble spread is considered to be a qualitative indicator of the forecast error if EnKF works well [10].

The final case (NO-SSHA) is the case 'dqc.m1p2' but with assimilation of only SST (RMCSST, AMSR, and MODIS-SST) designed to investigate roles of SST and sea surface height anomaly assimilations in the representation of the Kuroshio variation south of Japan in the present context. Table 2 summarizes the description of the all data assimilation experiments and another reference case of a simulation without any kind of data assimilation (NO-ASSIM).

Table 2. Description of model experiments.

Case	Quality Control (Equation (2))	Assimilated data
NO-ASSIM	-	-
NO-MODIS	m = 10, p = 10	RMCSST,AMSR-E,SSHA
mqc	m = 10, p = 10	RMCSST,AMSR-E,MODIS,SSHA
5degerr	m = 10, p = 10 (observation error = 5 °C)	RMCSST,AMSR-E,MODIS,SSHA
m3p4	m = 3, p = 4	RMCSST,AMSR-E,MODIS,SSHA
m2p2	m = 2, p = 2	RMCSST,AMSR-E,MODIS,SSHA
m1p2	m = 1, p = 2	RMCSST,AMSR-E,MODIS,SSHA
m2	m = 2, p=10	RMCSST,AMSR-E,MODIS,SSHA
m1	m = 1, p = 10	RMCSST,AMSR-E,MODIS,SSHA
dqc.m2p2	m = 2sprd, p = 2sprd	RMCSST,AMSR-E,MODIS,SSHA
dqc.m1p2	m = sprd, p = 2sprd	RMCSST,AMSR-E,MODIS,SSHA
dqc.m2	m = 2sprd, p = 10	RMCSST,AMSR-E,MODIS,SSHA
dqc.m1	m = sprd, p = 10	RMCSST,AMSR-E,MODIS,SSHA
NO-SSHA	m = sprd, p = 2sprd	RMCSST,AMSR-E,MODIS

3. Results and Discussions

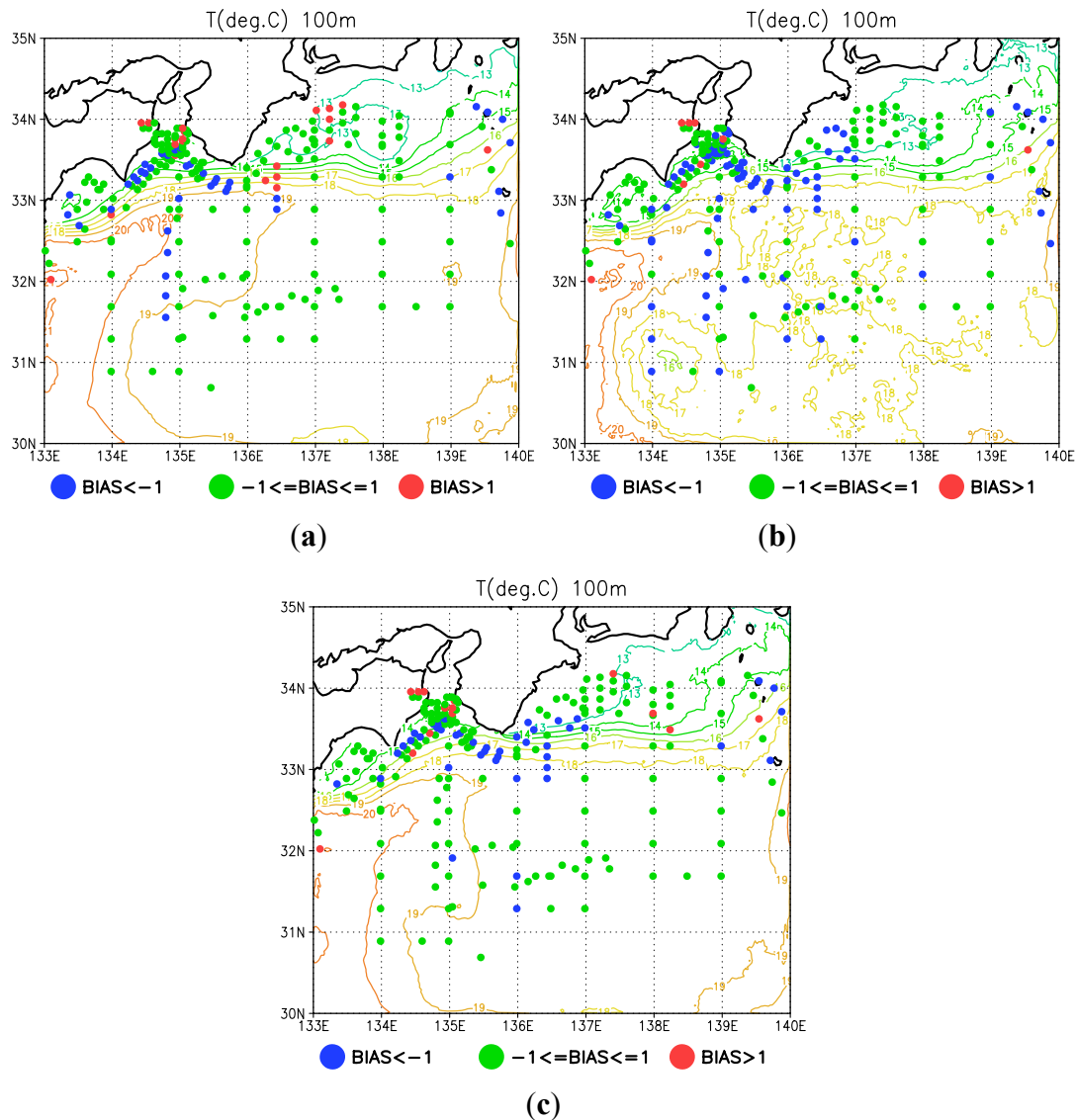### 3.1. Quality Control of MODIS-SST

Comparison of mean error (bias) for the *in situ* temperature profiles (Figure 3) exhibits that the assimilation of MODIS-SST, with the default quality control (mqc), actually causes lower temperature bias of the model product, in which the spatial averaged value (Table 3) is larger than those in the genuine simulation (NO-ASSIM) and the NO-MODIS case. An artificial cyclonic eddy due to the assimilation of erroneous low MODIS-SST appears around 31°N, 134°E (Figure 3(b)). The assimilation of MODIS-SST with the higher observation error (5degerr) reduces the low temperature bias but fails to remove the erroneous cyclonic eddy around 31°N, 134°E (not shown). All cases of the static (m3p4, m2p2, m1p2, m2, m1) and dynamics control (dqc.m2p2, dqc.m1p2, dqc.m2, dqc.m1) reduce the bias (Table 3). Reduction of T-RMSE in the cases with p = 10 (m2, m1, dqc.m2, dqc.m1) as compared to the cases with smaller p values (m3p4, m2p2, m1p2, dqc.m2p2, dqc.m1p2) suggests the validity of the default criterion (p = 10) for higher MODIS-SST than forecast SST. Table 3 also indicates that all the MODIS-SST cases except for the two dynamic control cases: dqc.m1 and dqc.m2 result in larger T-RMSEs than that (1.20) in the reference case of NO-MODIS. The dynamic quality control cases (dqc.m2p2, dqc.m1p2, dqc.m2, dqc.m1) reduce RMSEs as compared to the static quality control cases (m2p2, m1p2, m2, m1). Exclusion of SSHA (NO-SSHA) from the assimilation increases RMSE for *in situ* temperature profiles. Correlation to the assimilated MODIS-SST in the cases with the moderate criterion values tends to be generally higher than that in the cases with the strict criterion values. We conclude that two cases of the static and dynamics quality control: m2 and dqc.m2 are acceptable in terms of the balances among preferable conditions: higher correlation to MODIS-SST, and smaller bias and RMSE to *in situ* temperature and salinity.

Table 3. Averaged BIAS and RMSE of model experiments for the *in situ* temperature and salinity profiles.

Case	T-BIAS (°C), S-BIAS(psu)	T-RMSE (°C), S-RMSE(psu)	Correlation with Assimilated MODIS-SST
NO-ASSIM	−0.81, −0.039	1.83, 0.20	0.76*
NO-MODIS	−0.24, +0.012	1.20, 0.16	0.84*
mqc	−1.00, −0.068	1.63, 0.19	0.86
5degerr	−0.75, −0.041	1.40, 0.17	0.85
m3p4	−0.56, −0.022	1.34, 0.19	0.85
m2p2	−0.46, −0.015	1.30, 0.18	0.86
m1p2	−0.12, +0.024	1.25, 0.19	0.85
m2	−0.29, +0.013	1.23, 0.18	0.86
m1	+0.03, +0.053	1.24, 0.20	0.84
dqc.m2p2	−0.49, −0.002	1.25, 0.17	0.86
dqc.m1p2	−0.19, +0.030	1.23, 0.18	0.84
dqc.m2	−0.35, +0.006	1.17, 0.17	0.83
dqc.m1	−0.05, +0.037	1.16, 0.17	0.80
NO-SSHA	−0.27, +0.030	1.28, 0.18	0.84

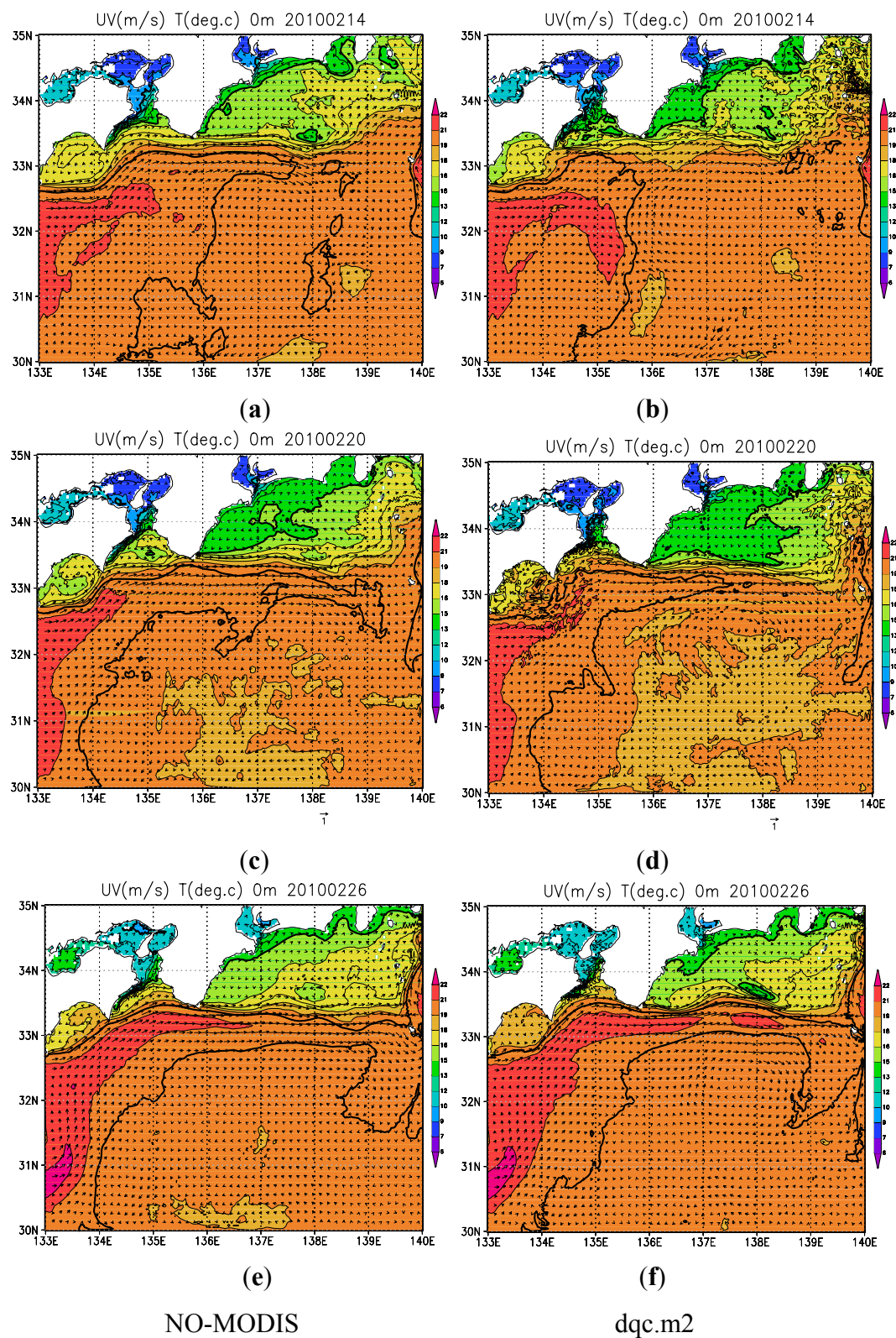*Correlation is calculated for MODIS-SST of which the deviation from forecast SST is smaller than 2 °C.

Figure 3. Contours indicate temperature at 100 m depth averaged for the period from 8 to 28 February 2010. Closed circles denote all positions of the *in situ* observations in which numbers were larger than 4 and their colors indicate mean error (bias) between the reproduced and observed *in situ* profiles. (**a**) NO-MODIS. (**b**) mqc. (**c**) dqc.m2.

(**a**)

(**b**)

(**c**)

3.2. Effects of High-Resolution SST

Comparison between the cases with and without MODIS-SST assimilation (Figure 4) indicates that MODIS-SST assimilation actually modifies the representation of the Kuroshio front variation by slightly changing the front position and adding smaller scales features, which are apparent in two regions: the Kii Channel and the Izu Islands (See Figure 1f for locations). In particular, representation of the front movement toward inside of the Kii Channel shown during the period [10] is improved as a result of MODIS-SST assimilation. Modification of the front is still found at the time (26 February 2010; Figure 4(f)) on which the number of MODIS-SST data was comparatively low due to the cloudy sky condition (Figure 1(f)). Note that no anomalous low temperature region is represented in the MODIS-SST assimilation products.
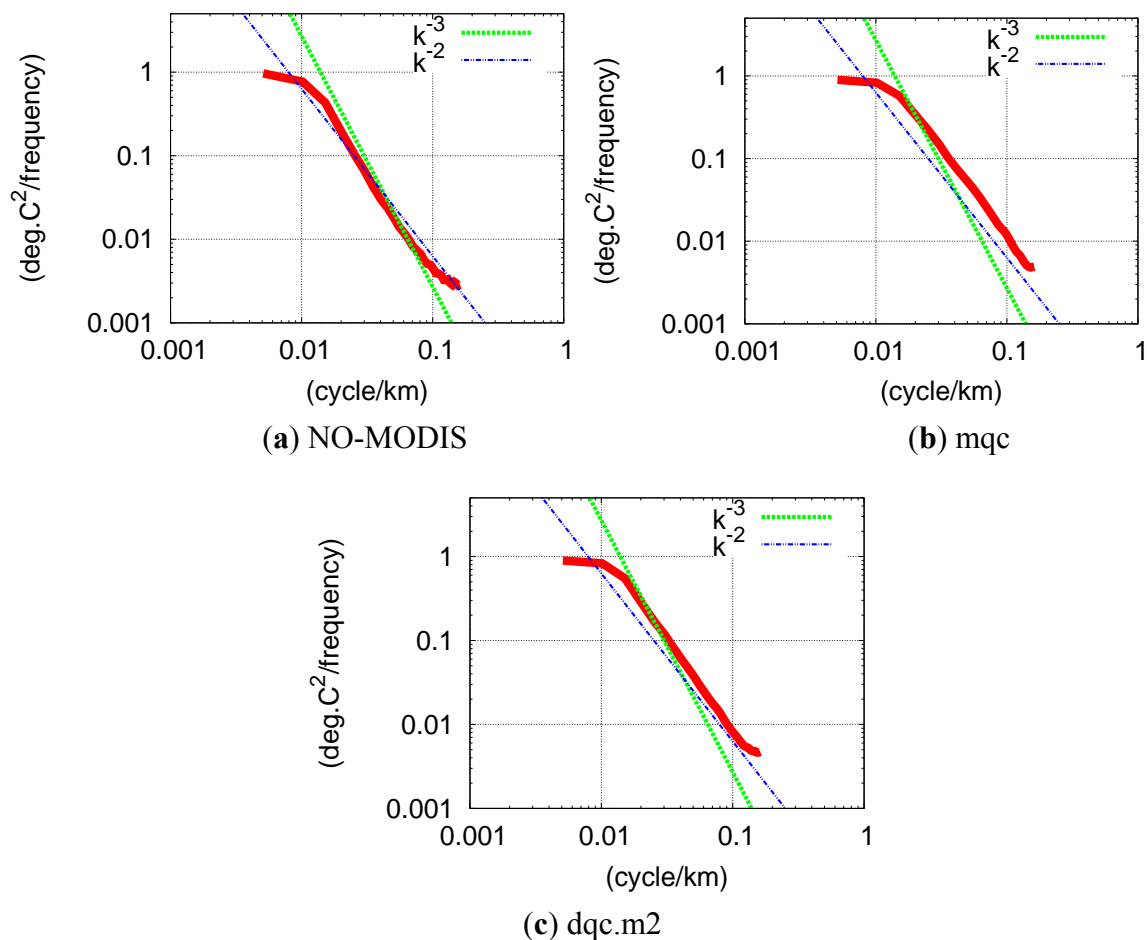
Figure 4. Snapshots of ensemble mean sea surface temperature (shade and contours) and flows (vectors). Interval of thin (thick) contours is 1 ℃ (5 ℃). (**Left**): NO-MODIS. (**Right**): dqc.m2. (**a**,**b**): 14 February 2010. (**c**,**d**): 20 February 2010. (**e**,**f**): 26 February 2010.

(a)   (b)

(c)   (d)

(e)   (f)

NO-MODIS   dqc.m2

To confirm changes in the representation of the front variability, resulting from MODIS-SST assimilation, we compare one-dimensional cross-shore wavenumber spectra of SST (Figure 5). The

NO-MODIS case (Figure 5(a)) shows a smoothed property with a ~k^{-3} slope, and the full assimilation of MODIS-SST (mqc) formally represents a more shallow ~k^{-2} slope (Figure 5(b)), which is a typical feature of the meso to sub-mesoscale transition [20,21]. However, the 1/36° (~3 km) grid of the present model may still be too coarse to keep the ~k^{-2} slope around 10 km scale (0.1 at the horizontal axis of Figure 5). The SST structure represented in the full assimilation of MODIS-SST (mqc) involves not only anomalous low temperature regions but also unrealistic noisy patterns (not shown). The assimilation with the stricter quality control (dqc.m2; Figure 5(c)) represents the ~k^{-2} slope in a wavenumber range from 0.02 (50 km) to 0.04 (25 km), which could be reasonably resolved by the model grid.

Figure 5. One-dimensional analysis SST spectra (solid curves) along cross-shore direction averaged in the model region south of 33°N and during the period from 8 February to 28 February, 2010. Spectra are normalized by their respective maximum values. The ~k^{-3} (~k^{-2}) slopes are displayed by dashed (dashed double-dotted) lines. (**a**) NO-MODIS. (**b**) mqc. (**c**) dqc.m2.

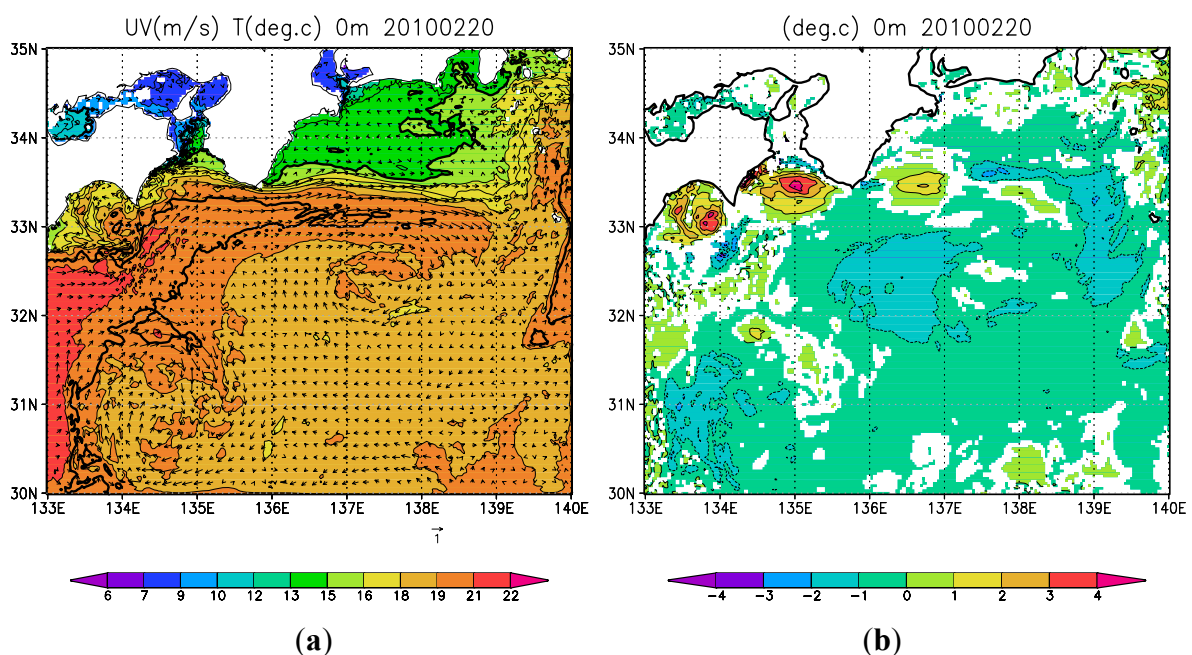(**a**) NO-MODIS

(**b**) mqc

(**c**) dqc.m2

The dynamic quality control is designed so that it facilitates modification of erroneous regions more than non-erroneous region. A snapshot from a static quality control case (m2; Figure 6(a)) shows similar patterns of the front variability to the dynamic quality control case (dqc.m2; Figure 4(d)) but shows noisy features that are not represented in the dynamic quality control case. To examine the difference between the static and dynamic cases in detail, we compare the impact signals of the two cases (Figures 6(b) and 7(a)). The impact signal (IS) is defined as:

$$IS \equiv \begin{cases} \bar{x}_w - \bar{x}_{w/o} & if \quad \left| \bar{x}_w - \bar{x}_{w/o} \right| \Big/ \sqrt{(Sprd_w^2 + Sprd_{w/o}^2)/(K-1)} > t_{95\%} \\ 0 & not \end{cases} \tag{3}$$

where $\bar{x}_w - \bar{x}_{w/o}$ is difference of ensemble mean variables between with (w) and without (w/o) the assimilation of the observation data: MODIS-SST in this case, K is ensemble size (=20), and $t_{95\%}$ is a critical t-distribution value of 95% significance with K-1 degree of freedom [22]. Comparison of Figure 6(b) and Figure 7(a) confirms that the static case (m2; Figure 6(b)) modifies SST more in open ocean than the dynamic case (dqc.m2; Figure 7(a)). Modification in the dynamic case is confined in regions with comparatively large magnitude of the ensemble spread (Figure 7) corresponding to potentially erroneous parts. The ensemble spread (Figure 7(b)) mainly represents variability associated with the Kuroshio northern edge front, recirculation of the Kuroshio, and winter channel fronts near the coast [10].

Figure 6. (**a**) As in Figure 4(d) except for the case 'm2'. (**b**) Impact Signal (IS; Equation (3)) of analysis SST in the case 'm2' on 20 February 2010 with and without MODIS-SST. Interval of contours is 1 °C.

(**a**)   (**b**)

Both of Figures 6(b) and 7(a) show that IS around the front regions represents un-isotropic shape along the front directions, suggesting the modification by EnKF consistent with the model dynamics. Forecast error covariance of SST between some grids around the fronts and surrounding grids (Figure 8) exhibit un-isotropic shape and spatial dependence that are closely related to the local model dynamics. We emphasize that EnKF assimilates MODIS-SST without over smoothing across the fronts owing to the effects of spatially varying forecast error covariance. We note that the forecast error covariance represented by EnKF is not only spatially variable but also highly variable in time (not shown), related to the time evolution of the model dynamics.

Figure 7. (**a**) As in Figure 6b except for the case 'dqc.m2'. (**b**) The ensemble spread of the case 'dqc.m2' for the EnKF analysis on February 20 2010. Shades (vectors) denote the spread of SST (surface current).
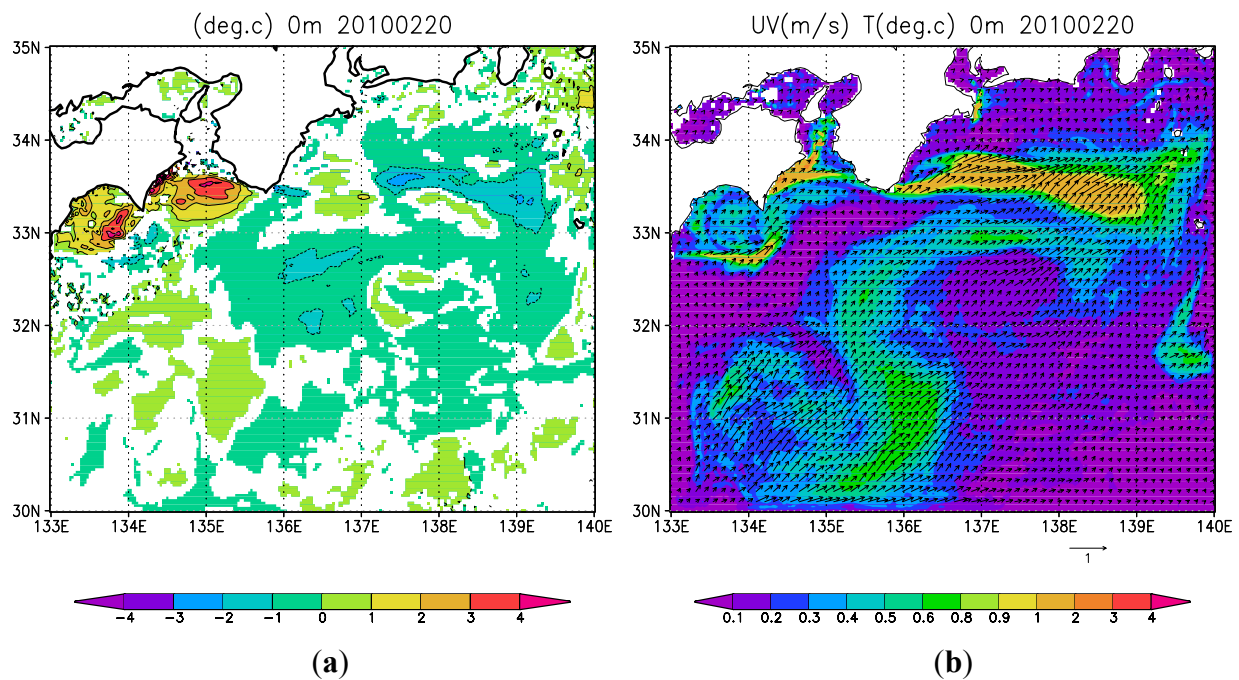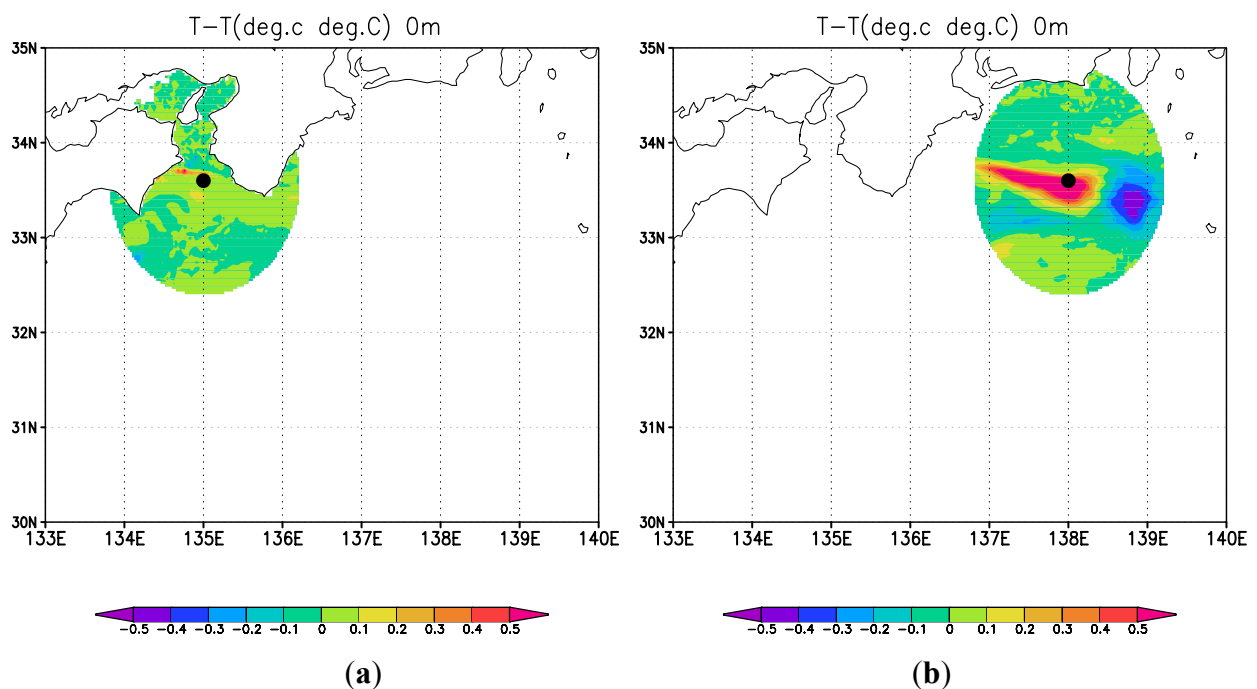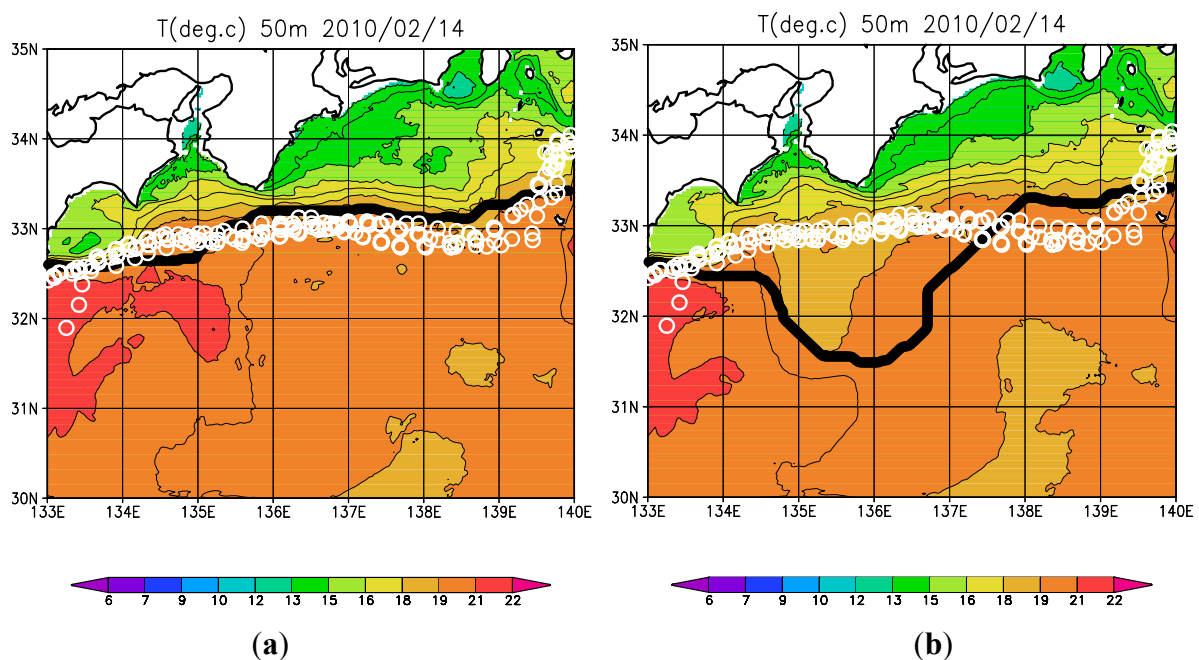

(**a**)

(**b**)

Figure 8. The forecast error covariance between SST at a target point and SST at surrounding grids on 20 February 2010. Values on the grids with distance from the target point larger than a localized scale ($dist_{zero} = \sigma_{obs}\sqrt{10/3}\,2 \sim 1.2°$; [10]) are not shown. Target points: (**a**) 33.6°N, 135°E. (**b**) 33.6°N, 138°E.

(**a**)

(**b**)

3.3. Roles of High-Resolution SST and Sea Surface Height Anomaly (SSHA) Data

A common understanding on roles of SST and SSHA in the ocean data assimilation is that the SST (SSHA) is effective for correction of the model variables near the shallower seasonal (deeper main) thermocline depth, e.g., [11]. To examine this issue in a new context of high-resolution SST and advanced data assimilation, we compare two dynamic control cases with and without (dqc.m1p2 and NO-SSHA) SSHA assimilation. Figure 9 indicates that the assimilation of only SST data fails to correct the Kuroshio axis position where no data are available due to existence of the clouds (Figure 1(b)). In addition, note that the SST assimilation is not very effective for detection of the Kuroshio axis position even in the eastern part of the model region where the data are available. RMS latitudinal differences of the modeled and observed Kuroshio axis positions during the simulation period from 8 February to 28 February 2010, are 0.45° (dqc.m1p2) and 0.63° (NO-SSHA), respectively. The assimilation of SSHA is necessary for detection of the Kuroshio path position that is closely related to the proper estimation of temperature around the main thermocline depth. The present study again confirms the finding of the previous studies.

Figure 9. Ensemble mean analysis temperature at 50 m depth (shade and contours) on 14 February 2010. (**a**) dqc.m1p2. (**b**) NO-SSHA. Thick contours denote the Kuroshio path positions evaluated from the ensemble mean flows at 50 m depth by tracking grids with the strongest kinetic energy at each longitude. Open circles represent the weekly mean observed path positions provided from the Japan Coast Guard. The duration of the weekly mean period was daily updated and then all position data including the target day in their weekly mean periods were plotted

(**a**)   (**b**)

3.4. Discussion

Figure 5 confirms that the 1/36° grid of the present model is coarser than a typical sub-mesoscale resolving grid distance of 1/100° [20], though the assimilation of MODIS-SST into the present model

partly contributes to the improvement in the representation of the meso to sub-mesoscale transition. We thus need to investigate the feasibility of the high-resolution SST data assimilation with horizontal resolution of around 1/100°. More studies using updated versions of the models with higher resolutions are required for further development of the MODIS-SST assimilation methods.

Probability distribution of the MODIS-SST data with lower temperature bias (Figure 2) could be considered as one of the non-Gaussian probability distributions. The present study practically deals with the observation data bias by using the data quality control prior to the EnKF assimilation. The basic framework of EnKF is designed on the basis of the assumptions of the Gaussian probability distributions of the model and data errors [13]. Recent advance of the data assimilation literature involves various types of extension toward the generalized filters suitable for the non-Gaussian type probability distributions, e.g., [23], which would be systematically used for the MODIS-SST data assimilation in the future.

The present study demonstrates the feasibility of MODIS-SST data assimilation into the high-resolution ocean models. We need to conduct more experiments covering longer periods and different regions to obtain more reliable results, with validated by more *in situ* data. In addition, the feasibility of MODIS-SST data assimilation in more economical data assimilation frameworks including 3-dimensional variational assimilation, e.g., [24], should be examined in near future. The results reported here could be a reference for future advanced studies.

4. Conclusions

The high-resolution sea surface temperature data obtained from the Moderate Resolution Imaging Spectroradiometer are assimilated into the three-dimensional ocean circulation model of south of Japan using the Local Ensemble Transformation Kalman Filter. Anomalously low temperature data, which characterize a large part of the noise associated with the clouds, are excluded prior to the assimilation by adopting the quality control method comparing the data with the ensemble mean forecast values. Addition of the high-resolution sea surface temperature actually enhances the spatial variability of analysis sea surface temperature over 50 km to 25 km scales, which are reasonably resolved by the present model. Spatiotemporally varying error covariance allowed by the Kalman filter contributes to detecting the highly spatiotemporally variable surface front variability. The ensemble spread information provided by the ensemble Kalman filter could be used for the effective detection of the phenomena that are well simulated by the present model. It is confirmed that the assimilation of only satellite sea surface height anomaly data is more suitable for detection of the large scale subsurface structure associated with the main thermocline variation such as the position of the Kuroshio main axis than the assimilation of only sea surface temperature.

Conflict of Interest

The authors declare no conflict of interest.

References

1. Miyama, T.; Nonaka, M.; Nakamura, H.; Kuwano-Yoshida, A. A striking early-summer event of convective rainband persistent along the warm Kuroshio in the East China Sea. *Tellus A* **2012**, doi:10.3402/tellusa.v64i0.18962.
2. Hosoda, K.; Murakami, H.; Sakaida, F.; Kawamura, H. Algorithm and validation of sea surface temperature observation using MODIS sensors aboard Terra and Aqua in the Western North Pacific. *J. Oceanogr.* **2007**, *63*, 267–280.
3. Hosoda, K.: Algorithm for estimating sea surface temperature based on Aqua/MODOS global ocean data. 2. Automated quality check process for eliminating cloud contamination. *J. Oceanogr.* **2010**, *67*, 791–805.
4. Haines, S.L.; Jedlovec, G.J.; Lazarus, S.M. A MODIS sea surface temperature composite for regional applications. *IEEE Trans. Geosci. Remot. Sens.* **2007**, *45*, 2919–2927.
5. Everson, R.; Cornillon, P.; Sirovich, L.; Webber, A. An empirical eigenfunction analysis of sea surface temperatures in the western North Atlantic. *J. Phys. Oceanogr.* **1997**, *27*, 468–479.
6. Chu, P.C.; Tseng, H.-C.; Chang, C.P.; Chen, J.M. South China Sea warm pool detected in spring from the Navy's Master Oceanographic Observational Data Set (MOODS). *J. Geophys. Res.* **1997**, *102*, 15761–15771.
7. Alvera-Azcarate, A.; Barth, A.; Rixen, M.; Beckers, J.M. Reconstruction of incomplete oceanographic data sets using empirical orthogonal functions: Application to the Adriatic Sea surface temperature. *Ocean Model.* **2005**, *9*, 325–346.
8. Guan, L.; Kawamura, H. Merging satellite infrared and microwave SSTs: Methodology and evaluation of the new SST. *J. Oceanogr.* **2004**, *60*, 905–912.
9. Sakaida, F.; Kawamura, H.; Takahashi, S.; Shimada, T.; Kawai, Y.; Hosoda, K.; Guan, L. Research and development of the New Generation Sea Surface Temperature for Open Ocean (NGSST-O) product and its demonstration operation. *J. Oceanogr.* **2009**, *65*, 859–870.
10. Miyazawa, Y.; Miyama, T.; Varlamov, S.M.; Guo, X.; Waseda, T. Open and coastal seas interactions represented by an Ensemble Kalman Filter. *Ocean Dyn.* **2012**, *62*, 645–659.
11. Ezer, T.; Mellor, G.L. Data assimilation experiments in the Gulf Stream region: How useful are satellite-derived surface data for nowcasting the subsurface Fields? *J. Atmos. Ocean Tech.* **1997**, 1379–1391.

12. Takahashi, W.; Kawamura, H. Detection method of the Kuroshio front using the satellite-derived chlorophyll-a images. *Remote Sens. Environ.* **2005**, *97*, 83–91.

13. Evensen, G. Sequential data assimilation with a nonlinear quasigeostrophic model using Monte-Carlo methods to forecast error statistics. *J. Geophys. Res.* **1994**, *99*, 10143–10162.

14. Hunt, B.R.; Kostelich, E.J.; Szunyogh, I. Efficient data assimilation for spatiotemporal chaos: A local ensemble transform Kalman filter. *Physica D* **2007**, *230*, 112–126.

15. Jordi, A.; Wang, D.-P. sbPOM: A parallel implementation of Princenton Ocean Model. *Environ. Modell. Softw*. **2012**, *38*, 59–61.

16. Berntsen, J.; Oey, L.-Y. Estimation of the internal pressure gradient in σ-coordinate ocean models: comparison of second-, fourth-, and sixth-order schemes. *Ocean Dyn.* **2010**, *60*, 317–330.

17. Miyoshi, T.; Sato, Y.; Kadowaki, T. Ensemble Kalman Filter and 4D-Var intercomparison with the Japanese operational global analysis and prediction system. *Mon. Wea. Rev.* **2010**, *138*, 2846–2866.

18. McClain, E.P.; Pichel, W.P.; Walton, C.C. Comparative performance of AVHRR-based multichannel sea surface temperatures. *J. Geophys. Res.* **1985**, *90*, 11587–11601.

19. May, D.A.; Parmeter, M.M.; Olszewski, D.S.; McKenzie, B.D. Operational processing of satellite sea surface temperature retrievals at the Naval Oceanographic Office. *Bull. Amer. Meteor. Soc.* **1998**, *79*, 397–407.

20. Capet, X.; McWilliams, J.C.; Molemaker, M.J.; Shchepetkin, A.F. Mesoscale to submesoscale transition in the California Current System: Flow structure, eddy flux, and observational tests. *J. Phys. Oceanogr.* **2008**, *38*, 29–43.

21. Wang, D.-P.; Jordi, A. Surface frontogenesis and thermohaline intrusion in a shelfbreak front. *Ocean Model*. **2011**, *38*, 161–170.

22. Moteki, Q.; Yoneyama, K.; Shirooka, R.; Kubota, H.; Yasunaga, K.; Suzuki, J.; Seiki, A.; Sato, N.; Enomoto, T.; Miyoshi, T; Yamane, S. The influence of observations propagated by convectively coupled equatorial waves. *Quart. J. Royal Meteoro. Soc.* **2011**, *137*, 641–655.

23. Harlim, J.; Hunt, B.R. A non-Gaussian ensemble filter for assimilating infrequent noisy observations. *Tellus A* **2007**, *59*, 225–237.

24. Miyazawa, Y.; Zhang, R.; Guo, X.; Tamura, H.; Ambe, D.; Lee, J.-S.; Okuno, A.; Yoshinari, H.; Setou, T.; Komatsu, K. Water mass variability in the western North Pacific detected in a 15-year eddy resolving ocean reanalysis. *J. Oceanogr.* **2009**, *65*, 737–756.